POLITECNICO DI TORINO
Repository ISTITUZIONALE

Pressure and kinetic energy transport across the cavity mouth in resonating cavities

Original
Pressure and kinetic energy transport across the cavity mouth in resonating cavities / Bailey, P.; Abba', A.; Tordella, Daniela. - In: PHYSICAL REVIEW E, STATISTICAL, NONLINEAR, AND SOFT MATTER PHYSICS. - ISSN 1539-3755. - STAMPA. - 87:013013(2013), pp. 013013-1-013013-11. [10.1103/PhysRevE.87.013013]

Availability:
This version is available at: 11583/2375319 since:

Publisher:
APS The American Physical Society

Published
DOI:10.1103/PhysRevE.87.013013

Terms of use:

This article is made available under terms and conditions as specified in the corresponding bibliographic description in the repository

Publisher copyright

(Article begins on next page)

12 October 2024

Pressure and kinetic energy transport across the cavity mouth in resonating cavities

Peter Roger Bailey,[1,*] Antonella Abbá,[2] and Daniela Tordella[1,†]
[1]*Politecnico di Torino, Dipartimento di Ingegneria Aeronautica e Spaziale, Corso Duca degli Abruzzi 24, 10129 Torino, Italy*
[2]*Politecnico di Milano, Dipartimento di Matematica, Piazza Leonardo da Vinci 32, 20133 Milano, Italy*
(Received 27 July 2012; published 14 January 2013)

Basic properties of the incompressible fluid motion in a rectangular cavity located along one wall of a plane channel are considered. For Mach numbers of the order of 1×10^{-3} and using the incompressible formulation, we look for observable properties that can be associated with acoustic emission, which is normally observed in this kind of flow beyond a critical value of Reynolds number. The focus is put on the energy dynamics, in particular on the accumulation of energy in the cavity which takes place in the form of pressure and kinetic energy. By increasing the external forcing, we observe that the pressure flow into the cavity increases very rapidly, then peaks. However, the flow of kinetic energy, which is many orders of magnitude lower than that of the pressure, slowly but continuously grows. This leads to the pressure–kinetic energy flows ratio reaching an asymptotic state around the value 1000 for the channel bulk speed Reynolds number. It is interesting to note that beyond this threshold when the channel flow is highly unsteady—a sort of coarse turbulent flow—a sequence of high and low pressure spots is seen to depart from the downward cavity step in the statistically averaged field. The set of spots forms a steady spatial structure, a sort of damped standing wave stretching along the spanwise direction. The line joining the centers of the spots has an inclination similar to the normal to the fronts of density or pressure waves, which are observed to propagate from the downstream cavity edge in compressible cavity flows (at Mach numbers of 1×10^2 to 1×10^3, larger than those considered here). The wavelength of the standing wave is of the order of 1/8 the cavity depth and observed at the channel bulk Reynolds number, Re $\sim$ 2900. In this condition, the measure of the maximum pressure differences in the cavity field shows values of the order of 1×10^{-1} Pa. We interpret the presence of this sort of wave as the fingerprint of the noise emission spots which could be observed in simulations where the full compressible formulation is used. The flow is studied by means of a sequence of direct numerical simulations in the Reynolds number range 25–2900. This allows the study to span across the steady laminar regime up to a first coarse turbulent regime. These results are confirmed by the good agreement with a set of laboratory results obtained at a Reynolds number one order of magnitude larger in a different cavity geometry [M. Gharib and A. Roshko, J. Fluid Mech. **177**, 501 (1987)]. This leaves room for a certain degree of qualitative universality to be associated with the present findings.

DOI: 10.1103/PhysRevE.87.013013 PACS number(s): 47.15.Rq, 47.27.ek, 47.27.wj

I. INTRODUCTION

Cavity flows are recirculation zones that can be found in many natural and engineering contexts. A few instances in which cavity flows are of significant importance are streaming blood through the heart (atrial and ventricular cavities), cooling towers of computers, musical wind instruments, aerodynamics of road vehicles and trains, and sound or pressure wave absorption devices where ridges present an increased surface area compared to a flat profile. In the vast scientific literature concerning cavity flows, most attention has been paid to describe the presence of separation regions caused by a sudden change in geometry, and the concomitant induced vortex formation, either steady or unsteady. In this regard, among many others, the reader may consider the work of Le, Moin, and Kim [1] (in the following referred to as LMK), Yoshizawa [2,3], and Haigermoser *et al.* [4]. Rather than focusing on the details of the vortex dynamics, flow topology, and structure of the flow pattern that forms inside the cavity, in this work we consider a different approach based on the determination of scaling Reynolds number power laws for basic quantities, such as the kinetic energy and pressure. To build scaling laws it is necessary to have access to a data set where the flow field can be observed when systematically varying the control parameter. This kind of data set has not yet been made available in the open literature. One motivation of this study is to partly fill this need by determining the velocity and pressure incompressible fields in a typical cavity geometry. A second motivation is associated with the occurrence of the acoustic resonance of a cavity, which can be present in the channel bulk when the Mach number is nearly zero, Ma $\sim 1 \times 10^{-3}$, as in a flute or an organ pipe. A question remains: In this situation, where in any respect but the acoustic emission the flow is to be considered incompressible, is it possible to observe within the incompressible formulation any basic phenomenon that can be associated with the acoustic resonance?

The cavity is placed within the wall of a plane channel. The Reynolds number is varied from low values (order of 25) up to values corresponding to coarse turbulent configurations. In this way, by means of direct numerical Navier-Stokes simulations, we span the entire steady laminar regime up to the hypothetical asymptotic condition represented by statistically steady-state turbulent condition (which corresponds to a global Reynolds number based on the bulk velocity of main channel flow of 2900 and to a cavity Reynolds number based on the average value of the velocity modulus inside the cavity of about 1200).

*Present address: Novartis Pharma AG, Postfach, CH-4002 Basel, Switzerland.
†daniela.tordella@polito.it

 ©2013 American Physical Society

Physically, the focus is put on the existence of an asymptotic limit of the ratio between the flows of the pressure and the kinetic energy across the cavity mouth with respect to the Reynolds number. By varying the Reynolds number in the range ([25], 2900), a three order of magnitude drop was observed for this ratio, which, beyond a bulk Reynolds number a little above 1000, is also seen to approach a decaying asymptotic state. In the laboratory, the acoustic emissions are observed to appear in the Reynolds number range [1000, 2000].

To summarize, the basic question that prompted this investigation is: How much energy in the form of pressure can be accumulated in the cavity—a hollow space within the wall of the channel—when the intensity of the flow forcing rises? The forcing here is the streamwise pressure gradient dp/dx. An increase of the pressure gradient means an increase of the Reynolds number. What happens when, by increasing the Reynolds number, the peak value of the pressure flow into the cavity is surpassed?

For one part of the results obtained here, namely the momentum across the cavity mouth, a comparison with laboratory findings is available. We have observed very good agreement with the set of laboratory results obtained at a bulk Reynolds number of 24 000 in a cavity placed along the wall of an axisymmetric body flow [5].

This is an unconfined flow, very different from the channel flow. This fact leaves room for a certain degree of qualitative universality to be associated to the present findings. We have analyzed the cavity flow, with aspect ratio 4, in the steady laminar regime as well as in one low Reynolds number turbulent condition (Re = [25,2900]). The Reynolds number is based on the bulk velocity of the flow in the channel and on the half channel height h. In the turbulent case, the mean as well as the fluctuating transport is analyzed.

The derivation of the energy balance relation and the aims of this research are presented in Sec. II. A description of the numerical experiment is given in Sec. III. Results based on the mean flow can be found in Sec. IV, followed by the fluctuating component in Sec. V. The concluding remarks are presented in Sec. VI.

II. PHYSICAL SYSTEM: REPRESENTATION OF THE TRANSPORT ACROSS THE CAVITY MOUTH

Let us consider the balance equation for the kinetic energy per unit mass, $E = \frac{u_i u_i}{2}$:

$$\frac{\partial E}{\partial t} + \frac{\partial (u_i E)}{\partial x_i} = -\frac{1}{\rho}\frac{\partial (p u_i)}{\partial x_i} + \delta - \epsilon, \tag{1}$$

where u_i $(i = 1,3)$ is the component of the velocity vector $\mathbf{u}$, p the pressure, ρ the density, and μ the dynamic viscosity, and where

$$\delta = \frac{\mu}{\rho}\frac{\partial}{\partial x_j}\left[\left(\frac{\partial u_i}{\partial x_j} + \frac{\partial u_j}{\partial x_i}\right) u_i\right], \tag{2}$$

$$\epsilon = \frac{\mu}{\rho}\left(\frac{\partial u_i}{\partial x_j} + \frac{\partial u_j}{\partial x_i}\right)\frac{\partial u_i}{\partial x_j}, \tag{3}$$

are the viscous diffusion and dissipation, respectively.

In steady conditions, or in steady conditions in the mean condition when the flow is turbulent, the divergence of the kinetic energy and pressure flow is balanced by the viscous diffusion and dissipation,

$$\frac{\partial (\rho u_i E - p u_i)}{\partial x_i} = \rho (\delta - \epsilon). \tag{4}$$

In this study we focus on the transport across the mouth of the cavity seen as the exchange surface where the interaction of the channel and cavity flow take place. We introduce a numerical coefficient α to represent the pressure transport as some factor of the kinetic energy transport:

$$pv = \alpha \rho v E, \tag{5}$$

where v indicates the velocity component normal to the cavity mouth. The factor α is determined also for the turbulent flow configuration which was considered to verify the existence of a Reynolds asymptote. In the turbulent case, the transport relevant to the fluctuation field was also considered. This is represented by the factor α_t that can be determined by using statistical averages:

$$\langle p' v' \rangle = \alpha_t \rho \langle v' E' \rangle. \tag{6}$$

The ensemble averaging $\langle\,\rangle$ is used to decompose a quantity $f = F + f'$ into the mean $F = \langle f \rangle$ and the fluctuation around it, f'.

III. NUMERICAL METHOD

The numerical tool used in this study is a mimetic implementation of the Navier-Stokes equations [6,7]. The method uses mass and vorticity preserving, in the sense that a discrete form of the vorticity equation is derived naturally by the application of the rotation operator to the discrete momentum equation.

To derive vorticity preserving discretizations, a reformulation of the momentum equation is considered, based on the identities (see, e.g., Ref. [8])

$$\mathbf{u} \cdot \nabla \mathbf{u} = \boldsymbol{\omega} \times \mathbf{u} + \nabla E, \tag{7}$$

$$\Delta \mathbf{u} = \nabla(\nabla \cdot \mathbf{u}) - \nabla \times \boldsymbol{\omega}, \tag{8}$$

where $\boldsymbol{\omega} = \nabla \times \mathbf{u}$ denotes vorticity.

The Navier-Stokes equations are then written in the form

$$\frac{\partial \mathbf{u}}{\partial t} = -\boldsymbol{\omega} \times \mathbf{u} - \frac{1}{\rho}\nabla(p + E) - \frac{\mu}{\rho}\nabla \times \boldsymbol{\omega}, \tag{9}$$

$$\nabla \cdot \mathbf{u} = 0. \tag{10}$$

The equations are advanced in time using a fractional step method of the type used by Kim and Moin [9], combined with an explicit three step Runge-Kutta scheme [6].

A staggered discretization grid, following the marker and cell (MAC) approach [10], is employed. The discrete velocity components are located at the center of the cell faces, while all the scalar components (pressure and kinetic energy) are defined at the cell center.

In order to make uniform as much as possible all the numerical aspects when moving from the steady laminar to the turbulent, steady in the mean, flow, we used the same three-dimensional computational domain. This has penalized the duration of the laminar simulations but has allowed a smooth numerical transition between the two conditions.

TABLE I. Collocation points N_x, N_y, N_z, in x,y,z directions, respectively, used for different bulk Reynolds number (Re) simulations.

Re	$N_x \times N_y \times N_z$
25–500	$329 \times 220 \times 6$
600–1000	$329 \times 220 \times 42$
1200–2000	$329 \times 220 \times 74$
2900	$329 \times 343 \times 74$

Different grid resolutions were used depending on the Reynolds number, as reported in Table I. During the simulations, cyclic boundary conditions are applied in the transversal homogeneous z direction. At the walls, the no slip condition for the velocity and Neumann condition for the pressure are imposed. Stretched meshes are applied, to guarantee that the laminar sublayer is well resolved for all the Reynolds numbers. Whereas a parabolic profile was imposed at the inlet for the laminar cases, for the turbulent configuration nonsteady velocity profiles, obtained with a direct simulation of a periodic channel flow without cavity, were imposed. At the outlet an absorbing condition is applied in order to minimize the effects of the boundary on the interior of the field [11].

As the initial condition, for the laminar flows, the Poiseuille solution was used. For the turbulent case, the velocity field obtained by a direct numerical simulation (DNS) was imposed at the initial time in the channel, while the flow was at rest in the cavity.

The computational domain considered is that of a channel with a rectangular cavity on the lower wall; see scheme in Fig. 1. In Fig. 1 the cavity mouth is highlighted. Profiles of the flow properties are considered across this area. Note that in this coordinate system a negative v velocity would be from the channel center towards the cavity floor, thus into the cavity.

Reynolds numbers in the range $\mathrm{Re} \in [25,2900]$, based on the half height of the channel and the bulk velocity, were considered. The coarse turbulent flow $\mathrm{Re} = 2900$ corresponds to a wall units Reynolds number of 180 turbulent flow in the channel. Results presented here were normalized on the following conditions:

air at 20 °C and 1 bar,

dynamic viscosity $\mu = 1.82 \times 10^{-5}$ N s m^{-2},

density $\rho = 1.19$ kg m^{-3},

channel half height $h = 0.1$ m, and

$L_x = 1.257$ m, $L_z = 0.314$ m.

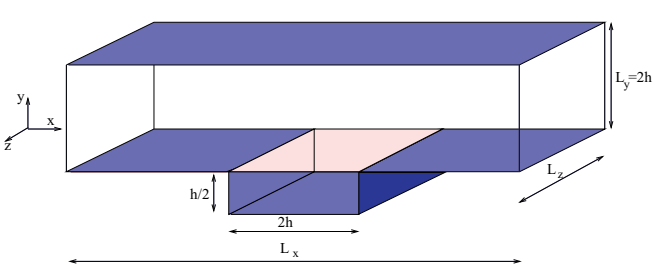

FIG. 1. (Color online) Scheme of the channel-cavity domain. Dimensions are defined with reference to the half channel height h. The cavity is located at the center. In the computational domain, L_x/h is $4\pi h$ and L_z/h is π.

An ambient pressure $p_a = 1$ atm (101 250 Pa) was taken at the channel inlet.

IV. PRESSURE AND KINETIC ENERGY TRANSPORT

Despite the fact that most flows in both engineering and nature are turbulent, the laminar cavity flow is still of significant importance. Howe [12] showed not only that laminar mean flows can induce oscillations, but that laminar flow resonances are often more intense. A laminar flow regime is also an important point from which to consider a wide range of Reynolds numbers for a study of the dynamics of a flow configuration. In both laminar and turbulent cavity flows, after separation at the upstream edge, the mean flow forms a vortex of the dimension of the cavity depth. Reattachment to the floor of the cavity depends on its aspect ratio. For a laminar cavity, reattachment is dependent on the Reynolds number and is typically of the order of 10 cavity depths downstream of the upstream edge. For a turbulent cavity this is less dependent on the Reynolds number and is widely accepted to be around six cavity depths downstream of the upstream edge [13–15]. The region between this reattachment point and the upstream edge is dominated by a large recirculation. For flows with cavity aspect ratio less than these values, except for Stokes flows at low Reynolds number, the cavity is likely to be "open," in which, after separating from the leading edge, reattachment takes place near the trailing edge. The whole cavity is then dominated by a recirculation region with, for higher Reynolds number, the principal eddy located close to the downstream edge.

We begin the description of the results by presenting in Fig. 2 an overview of the flow in the cavity for different Reynolds numbers: on the left-hand side the pressure field $(p-p_a)$ (in mPa) and the contour level for the spanwise vorticity component are represented, while on right-hand side the kinetic energy (in J) and velocity streamlines are shown. Since we want to give a qualitative picture of the flow, contour levels for the spanwise vorticity component and for the streamlines are not equally spaced and values for the best representation were selected. For the lowest Re here considered, 25, the cavity flow is almost "closed"; i.e., the flow almost reattaches to the floor of the cavity. On increasing Re, the principal eddy, the dominant vortical motion in the cavity, moves from the vicinity of the upstream edge to close to the downstream edge, and the secondary eddy increases in dimension.

For the turbulent case that we consider here (a turbulent channel flow with Reynolds numbers $\mathrm{Re} = 2900$ based on bulk flow, $R_\tau = 180$ based on wall friction velocity), all the quantities are averaged over the spanwise direction z and over a temporal interval of about 8 s, which corresponds to 16 bulk flow time scales ($\tau = 2h/U_{\mathrm{bulk}}$). In this situation [see Fig. 2(j)], the secondary eddy becomes about the same size as the principal eddy. Differently from the laminar cases, the pressure field in the cavity is controlled by the presence of both principal and secondary vortices.

In Fig. 3, a zoomed view of the pressure field close to the downward cavity step is shown. In the plane of the visualization, the x-y plane, a trace of a sheet stretched along the spanwise direction, where a pressure oscillation in space appears, can be noted. Since the image shows data averaged in time and space, along the spanwise direction, this sheet

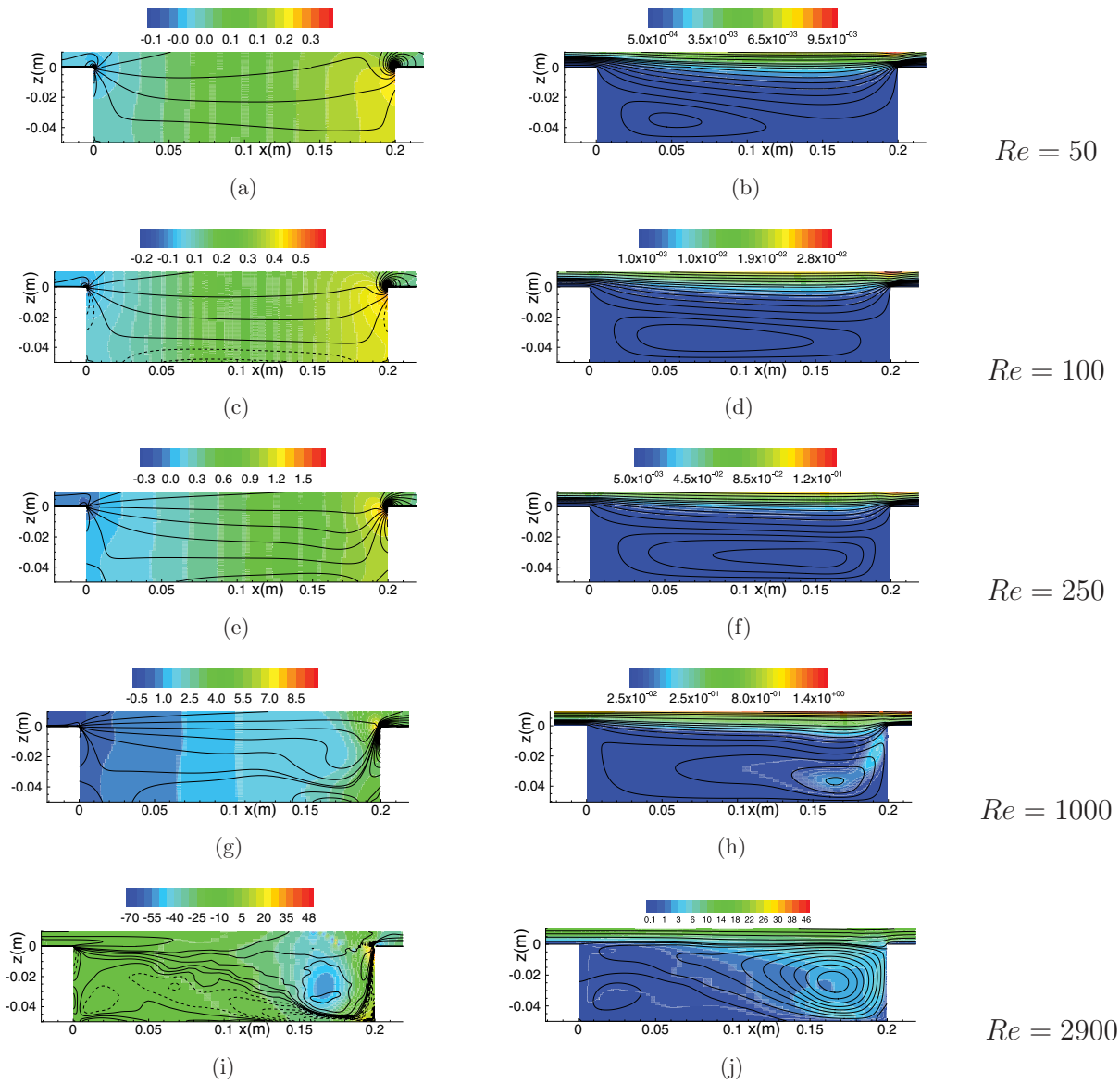

FIG. 2. (Color online) Flow visualization inside the cavity. Flows in the Re range [50,2900]. Laminar flows. (a, c, e, g) Pressure field $(p - p_a)$ (in mPa) and contour levels for the spanwise vorticity component, where p_a is the pressure at the channel inlet. (b, d, f, h) Kinetic energy (in J) and velocity streamlines. The averaged turbulent flow at Re = 2900 is represented in (i) distributions of the mean pressure $(p - p_a)$ and mean spanwise vorticity component and (j) mean kinetic energy distribution and mean velocity streamlines. The mean values are computed by averaging in time over 16 flow time scales and in space over the spanwise direction. The principal eddy tends to a position in the downstream half of the domain and the secondary eddy grows with Re. See Ref. [16].

can be interpreted as a kind of standing wave that departs from the high pressure spot visible on the surface of the downward cavity step. The sheet is backward inclined by about 26° with respect to main flow in the channel. The wavelength of the wave is of the order of 1/8 of the cavity depth (1/32 of the cavity width). In this condition, the measure of the maximum pressure difference inside the cavity shows a value of the order of 1×10^{-1} Pa, which in a sound wave could be roughly equivalent to a sound pressure level of 50–60 dB. We interpret the presence of this standing wave as the fingerprint of the noise emission which exists in flow configurations close to this one and that cannot be observed in this study since we are not dealing with the full compressible model. The interesting point here is, however, the fact that the incompressible formulation seems capable of capturing a signature of the acoustic production. It should be noted that the inclination angle of this sheet is in good agreement with the inclination of the normal to the contours of constant pressure visible near the rear wall in the aspect ratio 4 cavity visible in Fig. 18(b) of the study by Rowley, Colonius, and Basu [17], which concerns the behavior of self-sustained oscillations in two-dimensional compressible flow over a rectangular cavity. In this case, the Mach number is 0.6 and the cavity is in the wake mode configuration. The wake mode is characterized by a large-scale vortex shedding with Strouhal number independent of Mach number. It is interesting to see that the wake mode oscillation is similar in many ways to that reported by Gharib and Roshko [5] for incompressible flows with a laminar

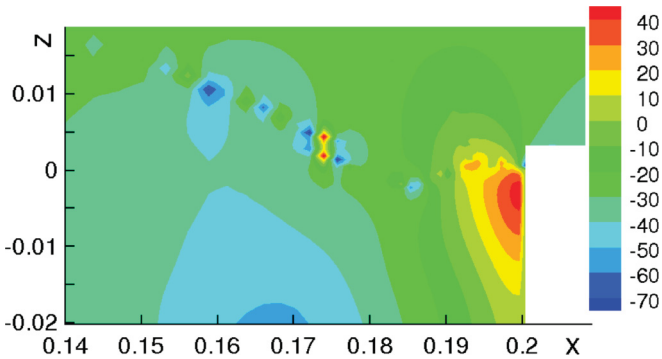

FIG. 3. (Color online) Expanded view of the pressure field in the downstream edge region at Re = 2900. A sequence of high and low pressure spots departs from the edge. The Mach number is of the order of 1×10^{-3}. The line joining the spot centers is backward inclined by about $-150°$, which is close to the inclination of the acoustic wave observed in the compressible simulations or laboratory observations with Mach numbers in the range 0.1–0.7 [17]. The average is carried out in time over 16 flow time scales and in space over the whole spanwise length of the computational domain.

upstream boundary layer. Also in our case the upstream flow is laminar and, in fact, our velocity fields have very good agreement with the available data by Gharib and Roshko [5], which are presented along the cavity mouth. This is explained below and shown later in Fig. 7.

Figure 4 shows the dimensioned streamwise pressure distribution in the channel and cavity for four Reynolds numbers. The profiles are taken along the bottom wall of

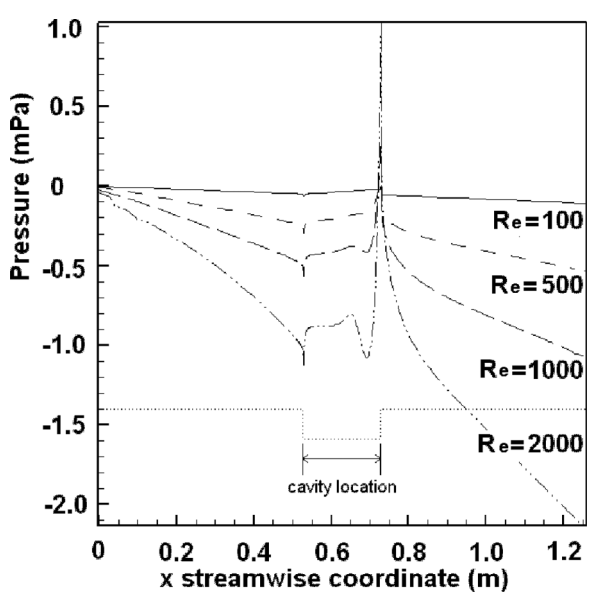

FIG. 4. Dimensioned streamwise pressure profiles at the level of the channel wall and cavity mouth for Re = 100, 500, 1000, and 2000. A constant pressure gradient is seen far from the cavity. Closer to the cavity this constant gradient is subject to a perturbation, with an increase in pressure just downstream of the separation point, a low over the location of the principal eddy for the higher Reynolds number cases, and a peak at the location of the downstream edge. The ordinate represents the pressure difference with respect to the ambient.

TABLE II. The resulting bulk velocity and pressure gradient in the channel, for different Reynolds numbers. Data built on a flow domain with dimensions $L_x = 1.257$ m, $h = 0.1$ m, and $L_z = 0.314$ m; see the scheme in Fig. 1.

U_{bulk} (mm/s)	Re	Pressure gradient (mPa/m)
3.8	25	−0.020865
7.6	50	−0.041730
15.3	100	−0.083461
22.9	150	−0.121591
30.6	200	−0.166922
38.2	250	−0.208652
45.9	300	−0.250383
61.2	400	−0.333844
76.5	500	−0.417305
122.3	800	−0.667687
152.9	1000	−0.834609
183.5	1200	−1.001531
229.4	1500	−1.251914
305.8	2000	−1.669218
443.4	2900	−9.826689
1681.9	11000	−77.423917

the channel and, in correspondence with the cavity, along the cavity mouth (the location of the cavity is shown in the diagram). It can be seen that as Re is increased, and when considering a given fixed flow geometry, the pressure gradient required to overcome losses at the channel wall is greater (see Table II). In the region of the cavity upstream edge, the pressure drops suddenly and then increases downstream of the separation point. Moving downstream the channel pressure gradient is perturbed by the flow structures within the cavity, more evidently for the cases Re = 1000 and Re = 2000 where a dip in the profile can be noted close to the downstream edge. At the downstream edge there is a sharp peak in the profile at the point where the flow stagnates.

By observing the flow properties at the cavity mouth, it can be seen from the profiles of the wall normal v velocity in Fig. 5 that there is a large area of low magnitude flow, mostly outflow, followed by a confined region with a higher magnitude inward velocity. For the laminar cases $500 < \text{Re} < 2000$ this large area is an outflow, whereas for the turbulent case the flow direction and magnitude oscillate, with a peak inflow flanked by two areas of outflow. For all these Reynolds numbers there then follows a high magnitude inflow into the cavity in the vicinity of the downstream edge. In the case of Re = 100, which corresponds to a partially open cavity case, the behavior is different. An outflow is apparent close to both the edges, with a large area of low velocity inflow between them. For details, see the inset in Fig. 5.

The mean kinetic energy per unit volume along the cavity mouth is shown in Fig. 6. This quantity is dominated by the streamwise velocity component, which is one order of magnitude greater than the wall normal velocity, with the spanwise component null in the laminar flow and on average in the turbulent flow.

It should be noted that these results agree with laboratory findings [5] related to a turbulent cavity flow with a different

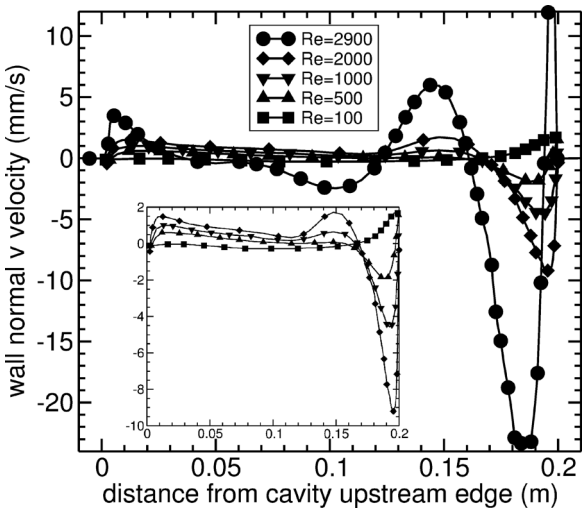

FIG. 5. Dimensioned v wall normal velocity across the mouth of the cavity. A large area of velocity outflow is followed by a more confined region of relatively high velocity inflow close to the downstream edge.

geometry and a Reynolds number about 10 times larger, a thing which highlights a good level of generality for our results (see Fig. 7). In particular, the experimental investigation concerned a flow over an axisymmetric cavity. In this work it was shown that self-sustained, periodic oscillations of the cavity shear layer are associated with a low cavity drag and can regulate the external mean shear layer to fix the stagnation point at the downstream corner.

We now turn our attention to forming the products which make up the transport terms. The product of the pressure and wall normal v velocity at the cavity mouth is depicted in Fig. 8(a) for cases Re = 100–2900. The profile very much takes its form from the cavity mouth velocity profile found in Fig. 5, with a low magnitude transport upstream and more confined high magnitude close to the downstream edge.

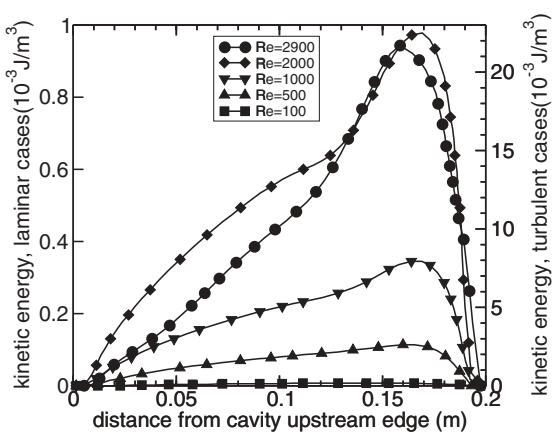

FIG. 6. Mean kinetic energy E per unit volume across the mouth of the cavity. E increases with Re with a scaling exponent which has been estimated as 1.4 for the laminar cases. When passing to the turbulent case, the mean kinetic energy, defined as $\langle E\rangle = \langle \rho \frac{u_i u_i}{2}\rangle$, is considered (diamonds). In this case the maximum $\langle E\rangle$ is an order of magnitude larger for a relatively small increment in Reynolds number, owing largely to the greater streamwise velocity in the region near the cavity mouth.

In Fig. 8(b) the kinetic energy transport along the mouth of the cavity is depicted. Most of the energy transfer takes place in the downstream half of the cavity. For Re > 500, it can be seen that the greatest magnitude transport occurs close to the downstream edge for the laminar cases. The peak in kinetic energy transport in the turbulent case can also be found in the same region. However, unlike in Fig. 5, where, passing from Re = 2000 to 2900, an increase of three times the maximum pressure transport is observed, a change in the ordinate scale is required for the energy transport case. Here, in fact, the maximum local transport in the turbulent case is almost two orders of magnitude greater than that in the highest Reynolds number laminar case.

In Fig. 9 the averages of the dimensioned pressure and kinetic energy transport across the cavity mouth are plotted as functions of Re. In our reference system (see Fig. 1), both the flows are negative, since the mean energy and pressure flow into the cavity. In Fig. 9, however, we plot the modulus of the flow. The kinetic energy transport can be seen to continually increase in magnitude with Re; indeed as Re is doubled the transport is more than doubled, which is a direct consequence of the increased kinetic energy entrained into the cavity mouth area as seen in the previous plots (Fig. 6). As can be seen in the figure, the energy flow grows according to two different interpolation curves. Up to Re = 1000, the growth scaling is that of a power law with an exponent close to 2. Beyond, the interpolation is logarithmic. The pressure transport reaches a maximum around Re = 1000, according to a logarithmic law, and is then seen to reduce if Re is increased further, according to a polynomial law. Figure 8(a) shows that the maximum local strength of the pressure transport increases with Re. Despite this it can be seen in Fig. 9 that the net transport of pressure remains relatively constant getting close to Re $\sim$ 1000. Increasing from this value, the rise in pressure outflow from the cavity is evidently greater than the increase in the inflow. Our interpretation is that in this range the acoustic emission appears. Since the cavity flow is a very confined flow, inside the cavity the development of many small scales is blocked. This reduces the dissipation action, and, to reach a steady state, an emission of energy in the form of acoustic waves is thus necessary. By considering now the ratio between the two mean transports for both the laminar and turbulent mean flow,

$$\alpha = \frac{pv}{Ev}, \quad \alpha_{2900} = \frac{\langle pv\rangle}{\langle Ev\rangle}, \tag{11}$$

which is shown as a function of Re in Fig. 10; one can see that for increasing Re this ratio tends to an asymptotic limit. The asymptotic ratio is more than four orders of magnitude lower than that measured at the very low bulk channel Reynolds number of 50 ($\mathrm{Re}_{\mathrm{cavity}}$ below 10). Moreover, the asymptote is reached where Re exceeds 1000 and it is beyond this value of Re that the first instances of unsteady flow can be expected. On incrementing Re further (values beyond 2000), the flow will become transitional, where pockets of agitated flow, or turbulent structures, will begin to appear (see, for example, Fig. 11). It is at this stage that the cavity flow starts to emit audible noise since, as discussed by Howe [18], these structures

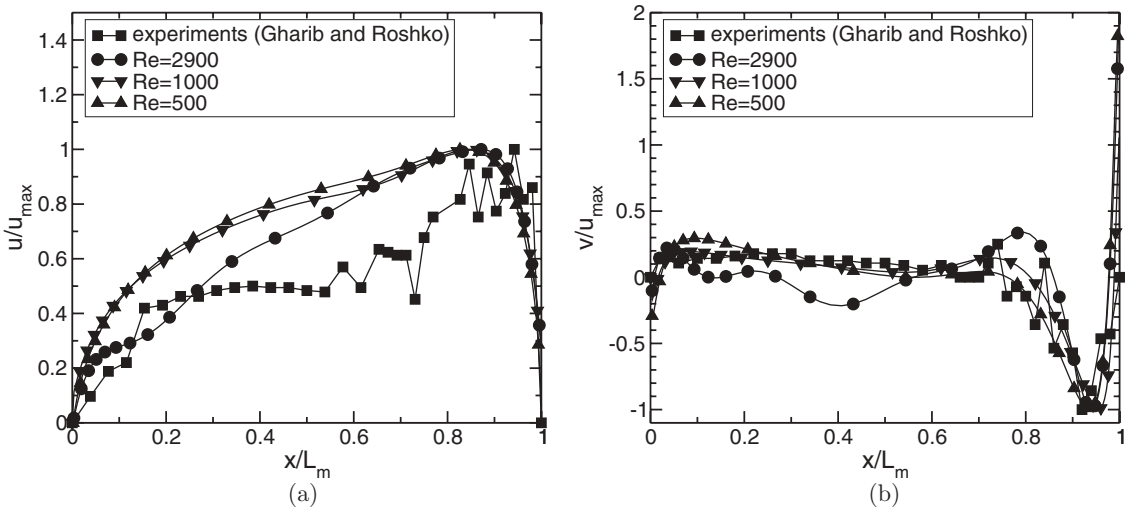

FIG. 7. Comparison of the streamwise and crosswise momentum along the cavity mouth with the laboratory results by Gharib and Roshko [5] obtained for a cavity placed along a boundary layer in cylindrical symmetry (Re = 24 000).

impinge on the downstream edge, causing a time disturbance to the pressure field. When the flow becomes turbulent the generation of the structures is more frequent and they usually have more energy. As a consequence, the pressure disturbance is greater. This set of phenomena—unsteadiness, transition, and turbulence—appears inside the asymptote regime here described.

In order to be able to better understand which is the Reynolds number seen by the flow in the cavity, a cavity Reynolds number, $\mathrm{Re}_{\mathrm{cavity}}$, has been defined, considering the mean parameters seen by the cavity. The mean velocity modulus in the cavity volume, $|\mathbf{u}|$, has been computed for each case, along with the mean dimension of the cavity, $l_{\mathrm{cavity}} = (\mathrm{length} + \mathrm{depth})/2 = 2.5h$, so that the cavity Reynolds number is defined as $\mathrm{Re}_{\mathrm{cavity}} = |\mathbf{u}| l_{\mathrm{cavity}}/\nu$. Table III presents the new range of Reynolds numbers alongside the global Re of the channel flow.

Visible from the table is the jump in values of the new $\mathrm{Re}_{\mathrm{cavity}}$ range. On moving from Re = 2000 to Re = 2900, i.e., incrementing Re by one half, we see almost an order of magnitude increase in $\mathrm{Re}_{\mathrm{cavity}}$. In the range $169 < \mathrm{Re}_{\mathrm{cavity}} < 1176$ the flow moves from the laminar to the turbulent regime (see Fig. 11). Thus considering that the cavity flow is a much confined configuration, where three walls act to suppress unsteadiness, an intermediate value in this range can be expected to be an approximate representation of the critical Reynolds number for the onset of a multiscale highly unsteady flow (a sort of very coarse turbulent flow). In laminar unsteady and turbulent situations, the mean flow energizes the fluctuating part. Thus where the mean flow is intense and fluctuations are present, as in this study where the flow region is close to the cavity trailing edge, the fluctuating structures acquire a lot of energy. See the experimental investigation by Gharib and Roshko [5] on the flow over an axisymmetric cavity that

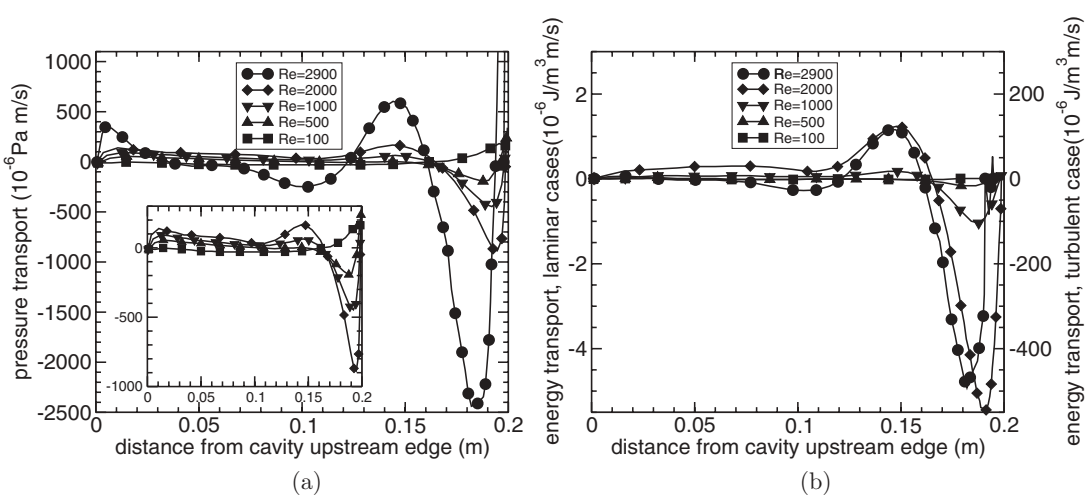

FIG. 8. (a) Dimensioned pressure transport and (b) kinetic energy transport profiles across the cavity mouth for the range $100 < \mathrm{Re} < 2900$ (all the flows are steady laminar, but Re = 2900 is the turbulent case). The inset omits the turbulent case. The pressure transport profiles resemble those of the velocity, where a low magnitude large area outflow is followed by a confined area of high magnitude inflow. Passing from the laminar to the turbulent case (diamond symbols), the local energy flow increases by two orders of magnitude.

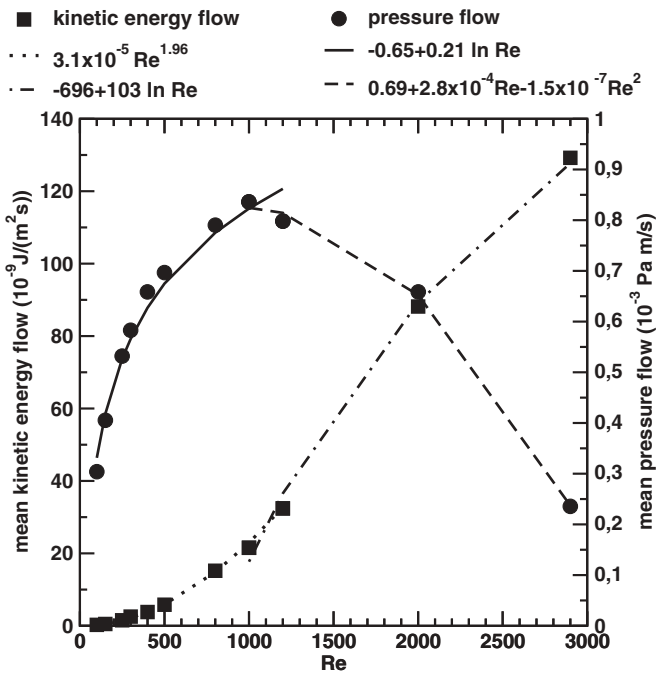

FIG. 9. Dimensioned absolute value of the pressure and kinetic energy transport across the cavity mouth versus Re. Within the adopted reference system, both the kinetic energy and pressure transports are always negative, i.e., into the cavity. Beyond Re $\simeq$ 1000 one can observe a change in regime, i.e., a polynomial decay for the pressure flow and a logarithmic growth for the energy flow. This produces an asymptotic exponential decay for the ratio of these quantities, as can be seen in Fig. 10. The mean energy (squares) and pressure (circles) transport before and after the Reynolds value of 1000 have been interpolated and are shown here. These two sets of curves were computed through the present direct numerical simulations by spanning the Reynolds number range [50, 2900]. For the energy transport we obtained $[3.1 \times 10^{-5}\mathrm{Re}^{1.96}]$ (dotted curve) and $[-696 + 103 \ln \mathrm{Re}]$ (dot-dashed curve); and for the pressure transport, $[-0.65 + 0.21 \ln \mathrm{Re}]$ (solid curve) and $[0.69 + 2.8 \times 10^{-4}\mathrm{Re} - 1.5 \times 10^{-7}\mathrm{Re}^2]$ (dashed curve).

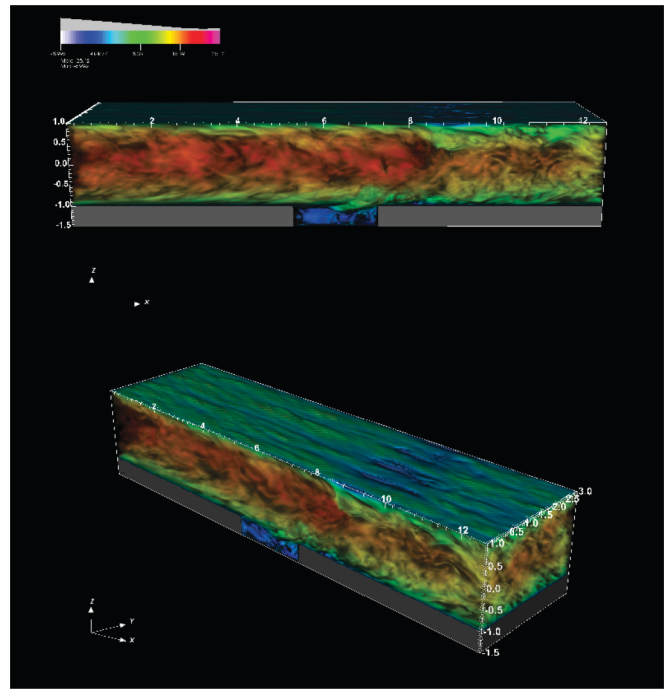

FIG. 11. (Color online) Three-dimensional visualization of the streamwise velocity component inside the turbulent channel-cavity flow. Bulk Reynolds number, Re = 2900. Reynolds number based on the averaged cavity dimensions and velocity modulus inside the cavity, $\mathrm{Re}_{\mathrm{cavity}} \sim 1200$. The lower velocity intensity and comparatively narrower range of scales inside the cavity should be noticed.

shows self-sustained, periodic oscillations of the cavity shear layer. Self-sustaining oscillations of high-Reynolds-number incompressible shear layers and jets incident on edges and corners are very common. These oscillations are frequently sources of narrow-band sound and are usually attributed to the formation of discrete vortices whose interactions with the edge or corner produce impulsive pressures that lead to the formation of new vorticity and complete a feedback cycle of

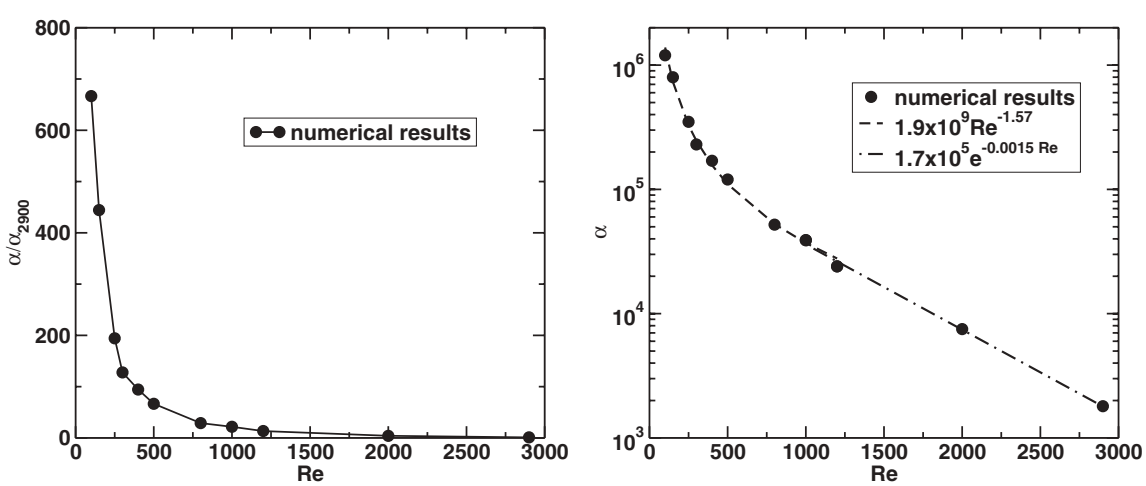

FIG. 10. The ratio α of pressure to kinetic energy flows initially decreases with $\mathrm{Re}^{-1.57}$, then sets to an exponential asymptote showing a tendency to reach the same state for flows of laminar and turbulent regimes. Indeed in the Reynolds number range where the asymptote is reached, the first instances of unsteady flow, instability, and acoustic emission should be expected (see, e.g., Refs. [12,18,19]).

TABLE III. Global channel Reynolds number (Re) versus cavity local Reynolds number ($\mathrm{Re}_{\mathrm{cavity}}$), based on the arithmetic mean of the cavity dimensions and on the average value of the velocity modulus inside the cavity.

Re	Bulk channel velocity (mm/s)	$\mathrm{Re}_{\mathrm{cavity}}$	Cavity velocity (mm/s)
100	15.3	16.0	0.962
250	38.2	32.5	1.956
1000	152.9	100.0	5.996
2000	305.8	169.0	10.120
2900	443.4	1176.0	70.560

operation. See, for instance, the works by Howe [12,18,20] where the influence of the mean shear on unsteady aperture flow, with self-sustained cavity oscillations, is discussed.

It should be noted that the set of laminar solutions produced in this work, $\mathrm{Re}_{\mathrm{cavity}}$ from 8 to 169, could also be used as basic steady flow for numerical perturbative studies of the cavity flow stability, in particular for the initial value problem of three-dimensional instability waves introduced into systems represented by the linearized Navier-Stokes flow field [19, 21–23]. The cavity flow is a recirculating flow and, as such, the standard perturbative scheme used for near parallel flow cannot be applied. However, due to the homogeneity in the streamwise and spanwise directions of the Poiseuille channel flow, perturbations in the form of longitudinal and transversal waves can be imposed to the flow above the cavity mouth, and, through it, conveyed to the cavity.

V. FLUCTUATING PRESSURE AND KINETIC ENERGY TRANSPORT

In both laminar and turbulent flows, separation, caused by a sudden change in geometry or a strong adverse pressure gradient, induces vortex formation, either steady or unsteady. The energy balance changes dramatically in these configurations when compared to flows which are predominantly unidirectional, such as the plane channel or boundary layer. Observing the kinetic energy transport rate statistics of turbulent wall bounded flows, it can be seen that the dominant terms are production and viscous dissipation, followed by the viscous diffusion and the turbulent transport. This differs in recirculation zones. For turbulent flows such as those downstream of back steps, Le *et al.* [1] and Yoshizawa [2,3] highlighted a redistribution of energy. Although still dominated by kinetic energy production and viscous dissipation, there is a rearrangement of the relative importance between the divergence of the pressure transport rate and the kinetic energy transport rate. Specifically the pressure transport rate represents a greater proportion of the kinetic energy transport. This was highlighted by Yoshizawa [3] on analyzing the DNS back-step flow of LMK [1] and trailing edge flows of Yao *et al.* [24]. The study of LMK [1] considered the boundary layer over a back step and thus a flow which is initially unidirectional before separating at a discontinuity in the flow geometry. Interestingly when analyzing the recirculating region downstream of the back step they note similarities

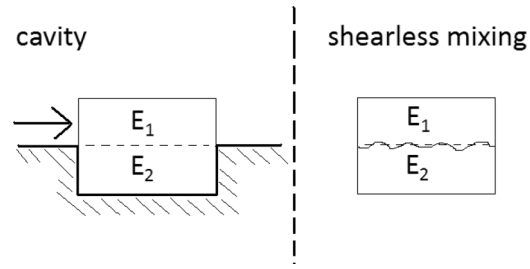

FIG. 12. Schemes of the interaction of turbulent regions with high ($E1$) and low ($E2$) kinetic energy content: (left) flow within and just outside the cavity in a volume of same extension and (right) flow across the shearless homogeneous isotropic turbulence mixing. For the turbulent cavity we measured $E1/E2 = 15.6$, whereas, for the shearless mixing, tests have been performed in the range for $10 \leqslant E1/E2 \leqslant 106$ (see Refs. [25,26]).

between the energy distribution found in the plane turbulent mixing layer.

Now turning our attention to the turbulent transport of energy and pressure across the cavity mouth, we can consider the cavity mouth as a plane surface between two regions of turbulent flow with differing energy contents. The flow in the channel just above the cavity mouth contains in fact more kinetic energy than the confined flow within the cavity (see Fig. 11). The ratio of transports between two turbulent fields with a significantly different content of kinetic energy was studied in a more fundamental configuration by Tordella *et al.* [25,26], where the interaction between two homogeneous isotropic turbulent fields (shearless mixing), differing in energy content, correlation length, or both, was investigated.

This configuration represents a very simple non homogeneous turbulent flow where, owing to the lack of the mean shear, the turbulent energy production is absent. Under this condition a relation between the pressure transport and the kinetic energy transport for varying energy ratios across the mixing has been found. For this turbulent mixing at values of the Taylor microscale Reynolds number of 45, 75, and 150, the coefficient α_t has been determined to be close to 0.37 for the range of energy ratios $E1/E2 \in [10, 10^6]$, and thus the pressure fluctuation transport is not dominated by the fluctuation kinetic energy transport.

Now comparing the previous result and that related to the turbulent cavity flow, where we have determined the energy ratio of the flow outside the cavity (region above the cavity mouth which has the same volume of the cavity; see Fig. 12) over that within, $E1/E2 = 15.39$, in the range of $\mathrm{Re}, \mathrm{Re}_{\mathrm{cavity}}$ here considered, and α_t has been determined to have a value of 0.58. It can be seen that also in the cavity flow case the fluctuation pressure transport is lower, albeit of the same order, than the fluctuation kinetic energy transport. This is a remarkably different behavior from that observed at the level of mean quantities. The turbulent transport appears to be less dependent on the Reynolds number and, also, not so highly dependent on the presence of a mean shear flow, as one would expect. However, the fluctuation pressure transport represents a slightly greater proportion of the fluctuation kinetic energy transport in the sheared cavity flow than in the shearless mixing.

VI. CONCLUSIONS

In this study, we considered the dynamics of very low Mach number cavity flows (Ma $\sim 1.0 \times 10^{-3}$), as observed from the point of view of the incompressible formulation. It is well known that, in this condition, cavity flows can emit acoustic waves and behave as a source of noise. On the one hand, to obtain information on the detail of the acoustic emission, one must consider the compressible formulation. On the other hand, if the acoustic emission was not present, nobody would consider adopting the compressible formulation to describe flows with a Mach number many orders of magnitude lower than 1.

In this work, we consider the cavity as an energy collector. Energy per unit volume can be stored in the cavity volume in two forms: kinetic energy and pressure. The energy and pressure flows take place across the cavity mouth.

We tried to answer the following question. Working inside the incompressible framework, is there any phenomenon that could be reasonably associated with pressure wave emission? The approach we used is very simple and basic. We considered a sequence of steady flow conditions rising from the low Reynolds number of the flow that feeds kinetic energy into the cavity. The sequence gets beyond the Reynolds number where the unsteady bifurcation is observed. It should be noted that the acoustic emission is usually described in association with the unsteady bifurcation. However, accurate sound emission measurements parametrized on a dense Reynolds number variation have not yet been reported in the literature. Thus, it is not yet known which is the Reynolds number threshold for sound emission.

We considered 14 laminar flow configurations and 1 turbulent flow configurations inside a plane channel with a cavity on one wall. The velocity, pressure, and kinetic energy properties along the mouth of the cavity were analyzed. It was seen that the kinetic energy along the cavity mouth scales with the bulk Reynolds number to the power of 1.4. The kinetic energy and pressure transport across the cavity mouth increase with Reynolds number up to the value 1000. Beyond this value a change of regime occurs, where the pressure flow decreases. The ratio between the pressure and energy flows always decreases with the channel bulk Reynolds number Re and, in the second regime, exhibits an asymptotic behavior represented by an exponential function with a negative exponent proportional to the Reynolds number.

Another observation is that, under the condition where the emission is surely present—a coarse turbulent flow configuration ($R_{2h} \sim 6.0 \times 10^3$, bulk Reynolds number in terms of the channel height)—a kind of plane standing pressure wave is generated near the backward facing step of the cavity. The wave is observed in the spatially and temporally averaged pressure field and is damped spatially. It has a wavelength of the order of 1/30 of the cavity length, and on the basis of an estimate of the amplitude of the root mean square of its damped fluctuation, a sound pressure level of about 60 dB would correspond.

On the contrary of what is generally observed for the turbulent transport, where, in near parallel flows, the pressure flow rate is dominated by the kinetic energy one, and, in recirculating regions, becomes of the same order, across the laminar or the turbulent cavity mouth, the pressure flow dominates by many orders the kinetic energy flow. However, in the near asymptotic condition we could observe, a recovery of the kinetic energy flow of about 700 times is seen.

In the turbulent case we observed, the pressure transport due to fluctuations is instead of the same order as that of the kinetic energy. In fact, the fluctuation pressure transport was found to be 0.58 the value of the kinetic energy transport, a figure which is not far from the value of 0.37 shown by the shear-free turbulent mixing.

A last outcome of this study is the accurate set of laminar solutions produced in the range of the Reynolds number based on the mean flow velocity inside the cavity, $\mathrm{Re}_{\mathrm{cavity}}$. By varying Re from the low value, Re = 25, to the value where the onset for the first instability can be expected, Re $\sim$ 2000, we see that $\mathrm{Re}_{\mathrm{cavity}}$ varies from 8 to 169. These numerical steady solutions can represent the basic flow for perturbation studies of the cavity flow stability. In particular, they can be used for the analysis of the initial value problem of three-dimensional perturbation waves introduced into the flow field described by the linearized Navier-Stokes model.

The numerical experiment is carried out taking into consideration physical dimensions that in principle can be easily reproduced in the laboratory. To promote a future comparison with laboratory data, we have therefore described all the results in terms of dimensioned quantities.

One last observation is that nowadays, compressible simulations at very small Mach number values, found in common nonaeronautical applications (that is, Ma $\sim 10^{-3}$), become feasible with the massively parallel machines, of course at the cost of translating the numerical codes to the highly distributed kind of parallelization. In this way, the details of the energy release by pressure waves could be obtained: one could measure the wavelength, verify the wavelength-frequency relationships, observe the evolution of the shape of the wave front, and determine the amount of energy released by pressure waves. And, very importantly, leaving aside the generation and propagation of the acoustic wave, one could verify which part of the physics of the system remains the same as seen in the incompressible formulation.

ACKNOWLEDGMENTS

We wish to acknowledge support of the CINECA supercomputing center. This research project has been supported by the AeroTranet Marie Curie Early Stage Research Training Fellowship of the European Community's Sixth Framework Programme under Contract No. MEST CT 2005 020301.

[1] H. Le, P. Moin, and J. Kim, J. Fluid Mech. **330**, 349 (1997).
[2] A. Yoshizawa, J. Phys. Soc. Jpn. **51**, 2326 (1982).
[3] A. Yoshizawa, Phys. Fluids **14**, 1736 (2002).
[4] C. Haigermoser, L. Vesely, M. Novara, and M. M. Onorato, Phys. Fluids **20**, 105101 (2008).
[5] M. Gharib and A. Roshko, J. Fluid Mech. **177**, 501 (1987)

[6] A. Abbà and L. Bonaventura, Int. J. Numer. Methods Fluids **56**, 1101 (2008).
[7] J. Hyman and M. Shashkov, SIAM J. Numer. Anal. **36**, 788 (1999).
[8] A. Chorin and J. E. Marsden, *A Mathematical Introduction to Fluid Mechanics* (Springer-Verlag, Berlin, 1993).
[9] J. Kim and P. Moin, J. Comp. Phys. **59**, 308 (1985).
[10] F. H. Harlow and J. E. Welsh, Phys. Fluids **8**, 2182 (1965).
[11] A. Abbà, R. Bucci, C. Cercignani, and L. Valdettaro, in *Small-Scale Structures in Three-Dimensional Hydro and Magnetohydrodynamic Turbulence*, edited by M. Meneguzzi, A. Pouquet, and P.-L. Sulem, Lecture Notes in Physics, Vol. 462 (Springer, Berlin, 1995), pp. 231–237.
[12] M. S. Howe, J. Fluid Mech. **330**, 61 (1997).
[13] S. N. Sinha, A. K. Gupta, and M. M. Oberai, AIAA J. **20**, 370 (1982).
[14] R. Camussi, G. Guj, and A. Ragni, J. Sound Vibrat. **294**, 177 (2006).
[15] P. J. Morris, *Short Course in General and Computational Aeroacoustics* (Universita' degli Studi Roma Tre, Rome, 2007).
[16] See Supplemental Material at http://link.aps.org/supplemental/10.1103/PhysRevE.87.013013 for detailed panels with quantitative information on the streamline function and vorticity contour values.
[17] C. Rowley, T. Colonius, and A. Basu, J. Fluid Mech. **455**, 315 (2002).
[18] M. S. Howe, J. Sound Vibrat. **273**, 103 (2004).
[19] G. A. Brès and T. Colonius, J. Fluid Mech. **599**, 309 (2008).
[20] M. S. Howe, J. Fluid Mech. **109**, 125 (1981).
[21] P. J. Schmid, Annu. Rev. Fluid Mech. **39**, 129 (2007).
[22] S. Scarsoglio, D. Tordella, and W. O. Criminale, Phys. Rev. E **81**, 036326 (2010).
[23] S. Scarsoglio, D. Tordella, and W. O. Criminale, Stud. Appl. Math. **123**, 153 (2009).
[24] Y. F. Yao, T. G. Thomas, N. D. Sandham, and J. J. R. Williams, Theor. Comput. Fluid Dyn. **14**, 337 (2001).
[25] D. Tordella, M. Iovieno, and P. R. Bailey, Phys. Rev. E **77**, 016309 (2008).
[26] D. Tordella and M. Iovieno, Phys. Rev. Lett. **107**, 194501 (2011).